RESEARCH ARTICLE | JULY 27 2022

Effects of doping, hydrostatic pressure, and thermal quenching on the phase transitions and magnetocaloric properties in Mn₁-xCoxNiGe **⊘**

Tej Poudel Chhetri ■ 💿 ; Jing-Han Chen 💿 ; Anthony T. Grant; David P. Young; Igor Dubenko; Saikat Talapatra; Naushad Ali; Shane Stadler



Check for updates

J. Appl. Phys. 132, 045107 (2022) https://doi.org/10.1063/5.0100987

A CHORUS





Articles You May Be Interested In

Giant magnetocaloric effect in isostructural MnNiGe-CoNiGe system by establishing a Curie-temperature

Appl. Phys. Lett. (March 2013)

Magnetostructural transformation and magnetocaloric effect in MnNiGe_{1-x}Ga_x alloys

J. Appl. Phys. (October 2013)

Enhanced magnetocaloric effects in metastable phases of Mn_{1-x}Co_xNiGe generated through thermal quenching and high-pressure annealing

J. Appl. Phys. (February 2023)





Effects of doping, hydrostatic pressure, and thermal quenching on the phase transitions and magnetocaloric properties in Mn_{1-x}Co_xNiGe

Cite as: J. Appl. Phys. 132, 045107 (2022); doi: 10.1063/5.0100987 Submitted: 27 May 2022 · Accepted: 1 July 2022 ·







Tej Poudel Chhetri, ^{1,a)} 🔟 Jing-Han Chen, ¹ 🔟 Anthony T. Grant, ¹ David P. Young, ¹ Igor Dubenko, ² Saikat Talapatra, ² Naushad Ali,² and Shane Stadler¹

AFFILIATIONS

Published Online: 27 July 2022

- Department of Physics and Astronomy, Louisiana State University, Baton Rouge, Louisiana 70803, USA
- ²Department of Physics, Southern Illinois University, Carbondale, Illinois 62901, USA

ABSTRACT

The effects of doping, hydrostatic pressure, and thermal quenching on the phase transitions and magnetocaloric properties of the $Mn_{1-x}Co_xNiGe$ system have been investigated. Cobalt doping on the Mn site shifted the martensitic structural transition toward lower temperature until it was ultimately absent, leaving only a magnetic transition from a ferromagnetic (FM) to a paramagnetic (PM) state in the high-temperature hexagonal phase. Co-occurrence of the magnetic and structural transitions to form a first-order magnetostructural transition. tion (MST) from the FM orthorhombic to the PM hexagonal phase was observed in samples with 0.05 < x < 0.20. An additional antiferromagnetic-ferromagnetic-like transition was observed in the martensite phase for 0.05 < x < 0.20. An additional antiferromagnetic-ferromagnetic-like transition was observed in the martensite phase for 0.05 < x < 0.10, which gradually vanished with increasing $\frac{8}{2}$. Co concentration (x > 0.10) or magnetic field (H > 0.5 T). The application of external hydrostatic pressure shifted the structural transition to $\frac{80}{100}$ lower temperature until an MST was formed in samples with x = 0.03 and 0.05, inducing large magnetic entropy changes up to $-80.3 \,\mathrm{J\,kg}^{-1} \,\mathrm{K}^{-1}$ (x = 0.03) for a 7-T field change under 10.6-kbar pressure. Similar to the effects of the application of hydrostatic pressure, an MST was formed near room temperature in the sample with x = 0.03 by annealing at high temperature (1200 °C) followed by quenching, resulting in a large magnetic entropy change of $-56.2 \,\mathrm{J\,kg^{-1}\,K^{-1}}$. These experimental results show that the application of pressure and thermal quenching, in addition to compositional variations, are effective methods to create magnetostructural transitions in the MnNiGe system, resulting in large magnetocaloric effects.

Published under an exclusive license by AIP Publishing. https://doi.org/10.1063/5.0100987

I. INTRODUCTION

Magnetostructural transition (MST), i.e., a coupling between magnetic and structural transitions, in magnetic materials is often associated with interesting magnetoresponsive effects, such as magnetic shape memory effects, ^{1,2} magnetocaloric effects (MCEs), ^{3–5} magnetoresistance phenomena, ^{6,7} etc. Among these, magnetocaloric effects (MCEs) have been the subject of intensive investigations over the past two decades because of their potential applications in magnetic cooling systems. These technologies have emerged as possible alternatives to the widely used, conventional vapor-compression cooling systems due to their superior efficiency and environmental friendliness. Magnetic materials that possess large MCEs are sought as potential candidates for such cooling systems. Over the past few

decades, numerous materials have been discovered as possible magnetic working materials, including $Gd_5(Si_2Ge_2)$, $La(Fe,Si)_{13}$ -based compounds, $^{8-10}$ Fe_2P -based alloys, 11,12 Ni-Mn based Heusler alloys, 13-19 and MnTX (T = transition metals and X = Ge, Si) systems.^{20–23} However, the magnetocaloric performances of these materials still need to be improved for the realization of an efficient magnetic refrigerator that operates at room temperature. Therefore, the development of effective methods to enhance the MCEs of existing materials or the discovery of new ones is highly desirable from an application point of view, and their investigation has been a global effort.

Among the aforementioned materials, MnTX (T = Ni, Co, and X = Si, Ge) systems have attracted considerable attention due to their pronounced MCEs resulting from a first-order

a)Author to whom correspondence should be addressed: tpoudel@lsu.edu

magnetostructural transition and accompanying large volume expansion/contraction. One member of this material family is MnNiGe, which undergoes a martensitic structural transformation from a Ni₂In-type hexagonal structure (P6₃/mmc) to a TiNiSi-type orthorhombic structure (*Pnma*) at temperature $T_{\rm M} = 470 \, \rm K$ and a magnetic transformation from a paramagnetic (PM) state to a spiral antiferromagnetic (AFM) state at a Néel temperature of $T_N = 346 \text{ K}$ while cooling.²⁴⁻²⁶ It undergoes an additional magnetic transformation from a simple spiral AFM to a cycloidal spiral AFM in the martensite phase upon further cooling. 27,28 Given that the magnetic and crystallographic stabilities in the MnTX systems are highly dependent on the covalent bonding between the T and X atoms, and on the interatomic distance between neighboring Mn atoms, 29,30 the phase transitions and magnetic exchange interactions in MnNiGe can be manipulated by elemental substitutions, 29,31-35 isostructural alloying, 36,37 and stoichiometric variations.³⁸ For example, a first-order MST from the PM hexagonal to the FM orthorhombic phase during cooling has been observed in MnNiGe when Mn is substituted by Fe.²⁹ Also, an MST from the FM hexagonal to AFM orthorhombic phases has been reported in off-stoichiometric Mn_{1,9-x}Ni_xGe systems.

Rather than changing the chemical composition, physical pressure and thermal treatments can also be used to manipulate the phase transitions.^{39–43} However, unlike the case of chemical modifications, few studies have been done to investigate the effects of pressure and thermal treatments on the MnNiGe system because of the low expectation of significant magnetocaloric effects. Therefore, the physical pressure-induced, or thermal treatment-induced, enhancement of the MCE has rarely been reported. Generally, materials undergoing MSTs with large volume changes are more sensitive to external stimuli, such as hydrostatic pressure, stress, heat treatment, etc. Previous investigations have shown that an MST with a considerable volume change can be established in Mn_{1-x}Co_xNiGe if Mn is substituted by Co atoms with $x \ge 0.10^{36}$ However, the impact of low Co-doping (x < 0.10) on the phase transitions (magnetic and structural transitions) remains unclear. Owing to a large volume change at the transition, the application of hydrostatic pressure and/or thermal processing can cause a change in lattice ordering, leading to a modification in the magnetocaloric properties in $Mn_{1-x}Co_xNiGe$, which are yet to be explored.

In the present work, we have explored the effect of Co-doping on the phase transitions of MnNiGe and constructed a comprehensive magnetic and structural phase diagram as a function of Co concentration. Furthermore, we demonstrated that magnetostructural coupling can be established in Mn_{1-x}Co_xNiGe through the application of hydrostatic pressure and/or thermal processing. The application of hydrostatic pressure resulted in the formation of MSTs in samples with x = 0.03 and 0.05, which significantly enhanced the magnetic entropy changes near room temperature. Moreover, magnetostructural coupling was realized over a wide temperature range (\sim 50 K) in the sample with x = 0.03, when quenched from or above 900 °C, resulting in large magnetic entropy changes on the periphery of room temperature.

II. EXPERIMENTAL DETAILS

Polycrystalline samples with nominal compositions of $Mn_{1-x}Co_xNiGe$ (x = 0, 0.03, 0.05, 0.08, 0.10, 0.12, 0.15, 0.20, and

0.25) were prepared by melting the constituent elements with purities better than 99.9% in an RF induction furnace in an argon atmosphere. The as-cast samples were sealed in separate quartz tubes under high vacuum and annealed at 800 °C for 60h for homogeneity and slowly cooled to room temperature.

To investigate the effects of thermal treatment, we selected a sample with x = 0.03 as a source ingot for the subsequent sample preparation. About 1-2 g of the source sample were sealed in different quartz tubes under high vacuum and annealed separately at 800, 900, 1000, 1100, and 1200 °C for 24 h followed by quenching in a vessel of liquid nitrogen by submerging and breaking the quartz tubes. These samples were labeled as Q800, Q900, Q1000, Q1100, and Q1200, respectively. An unquenched (annealed at 800 °C) or slow-cooled sample of the source ingot was labeled as SC800.

The crystal structures of the samples were determined at room temperature using x-ray diffraction (XRD) employing Cu-Kα radiation. The caloric measurements were performed using a differential scanning calorimeter (DSC). The magnetization measurements were performed using a Magnetic Property Measurement System (MPMS) manufactured by Quantum Design within a temperature interval of 2-400 K and in applied magnetic fields up to 7 T. The measurements under hydrostatic pressure were carried out using a commercial Be-Cu cylindrical pressure cell, where Daphne 7373 oil was used as the pressure transmitting medium and Sn as a reference manometer, which has a critical temperature $T_c = 3.72 \text{ K}$ at ambient pressure. The magnitude of the applied pressure was evaluated by measuring the shift of the superconducting transition temperature of Sn.

III. RESULTS AND DISCUSSION

perature of Sn.

RESULTS AND DISCUSSION

In this section, we report on three methods used to couple the netic and structural transitions. These include (a) atomic submagnetic and structural transitions. These include (a) atomic submagnetic and structural transitions. These include (a) atomic substitution, (b) application of hydrostatic pressure, and (c) thermal $\frac{1}{80}$ quenching.

A. Effects of Co substitution

The x-ray diffraction (XRD) patterns of $Mn_{1-x}Co_xNiGe$ (x = 0, 0.03, 0.05, 0.08, 0.10, 0.12, 0.15, 0.20, and 0.25) samples measured at room temperature are shown in Fig. 1. According to these results, the samples with x = 0, 0.03, and 0.05 are crystallized in a TiNiSi-type orthorhombic structure at room temperature. The XRD pattern of the sample with x = 0.08 can be indexed primarily as a Ni₂In-type hexagonal structure with some peaks of the TiNiSi-type orthorhombic structure, suggesting that the structural transition temperature is near room temperature (meaning that the high- and low-temperature phases coexist at room temperature). In the samples with x = 0.10, 0.12, 0.15, 0.20, and 0.25, only the diffraction peaks of the Ni₂In-type hexagonal structure were observed. These results, together with magnetization measurements, indicate that the transition temperature from the hexagonal austenite to the orthorhombic martensite phases decreases gradually with increasing Co concentration in Mn_{1-x}Co_xNiGe, which is consistent with previously reported results.³⁶ Rietveld refinements were performed using General Structure Analysis System (GSAS) software, 44,45 and the lattice parameters of their major crystal structures obtained from these refinements are tabulated in Table I. The results show

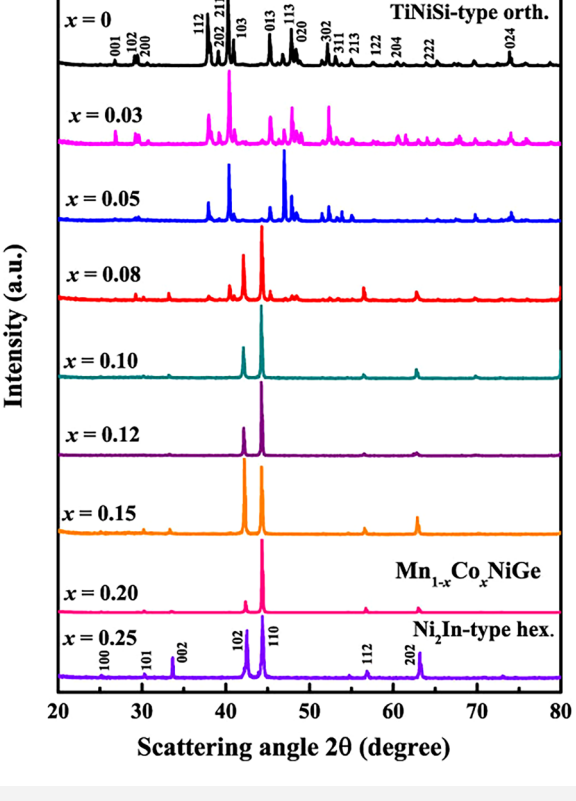


FIG. 1. Powder x-ray diffraction patterns of Mn_{1-x}Co_xNiGe for different Co concentrations (x) at room temperature. The crystal structure changes from a TiNiSi-type orth. for x = 0 to a Ni₂In-type hex. for x = 0.25.

that the lattice parameters and cell volume per formula unit in both the orthorhombic and hexagonal phases decrease with the increasing Co concentration. This reduction is the result of the replacement of the larger Mn atoms by smaller Co atoms.

To investigate the structural transitions in samples with x = 0and 0.03, which occur well above room temperature and are not

TABLE I. The lattice parameters and cell volumes per formula unit obtained from Rietveld refinements of the x-ray powder diffraction data of all Mn_{1-x}Co_xNiGe samples measured at room temperature

x	Major phase	a (Å)	b (Å)	c (Å)	Vol./f.u. (ų)
0	Orth.	6.052	3.760	7.101	40.40
0.03	Orth.	6.028	3.755	7.092	40.13
0.05	Orth.	6.026	3.754	7.091	40.10
0.08	Hex.	4.090	4.090	5.396	39.09
0.10	Hex.	4.089	4.089	5.386	38.99
0.12	Hex.	4.088	4.088	5.380	38.93
0.15	Hex.	4.086	4.086	5.374	38.85
0.20	Hex.	4.082	4.082	5.342	38.54
0.25	Hex.	4.079	4.079	5.318	38.32

observed in magnetization measurements using the MPMS, DSC measurements were performed upon heating and cooling with a ramp rate of 2 K/min. Figure 2 shows the baseline-corrected heat flow data as a function of temperature for both samples at ambient pressure. The well-defined exothermic and endothermic peaks arising from the latent heat of fusion were observed in the cooling and heating curves, indicating the forward and reverse structural transitions, respectively. The existence of a thermal hysteresis between the heating and cooling curves confirms that the transitions are first order. In the sample with x = 0, the forward and reverse structural transitions were found to occur at T = 482 and 502 K, respectively, with a hysteresis of $\Delta T = 20$ K. Meanwhile, those transition temperatures significantly decreased for x = 0.03and were observed at T = 380 and 398 K, respectively, with a hysteresis of $\Delta T = 18$ K.

Figure 3 shows the temperature-dependent magnetization measurements of all the samples performed at ambient pressure in an applied magnetic field of H = 0.1 T using zero-field-cooled (ZFC) and field-cooled-cooling (FCC) protocols. The magnetization results show that the sample with x = 0, i.e., stoichiometric MnNiGe, has a sharp peak due to the AFM-PM transition at $T_{\rm N}$ = 363 K. Additionally, a small peak associated with a spin reorientation-type transition was observed in the martensite phase at T = 265 K. In an earlier study, neutron powder diffraction measurements indicated that this transition corresponds to a transformation from a cycloidal spiral AFM phase to a simple spiral AFM phase during heating.²⁸ These transitions are consistent with the previously reported results for stoichiometric MnNiGe.²

When Co was introduced into the Mn site, the martensitic ctural transition shifted toward a lower temperature, stabilizathe high-temperature austenite phase. This phase stability may structural transition shifted toward a lower temperature, stabilizing the high-temperature austenite phase. This phase stability may

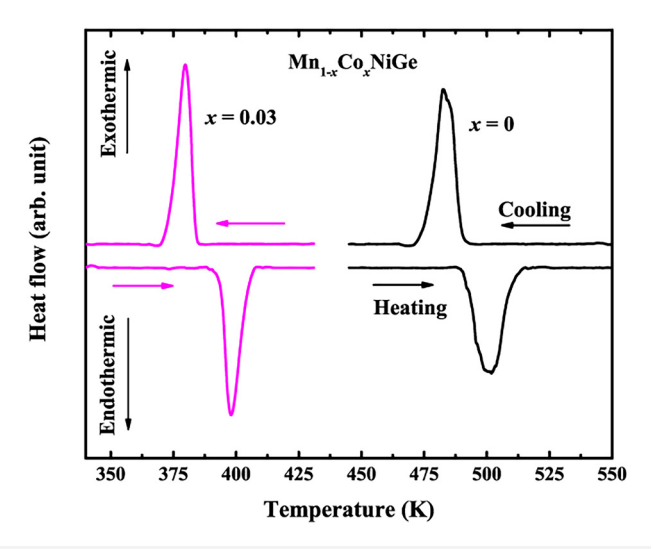


FIG. 2. The DSC curves for samples with x = 0 and 0.03 with a scan temperature rate of 2 K/min. The right- and left-pointing arrows indicate the direction of the heating and cooling scans, respectively. The curves have been corrected for baseline drift.

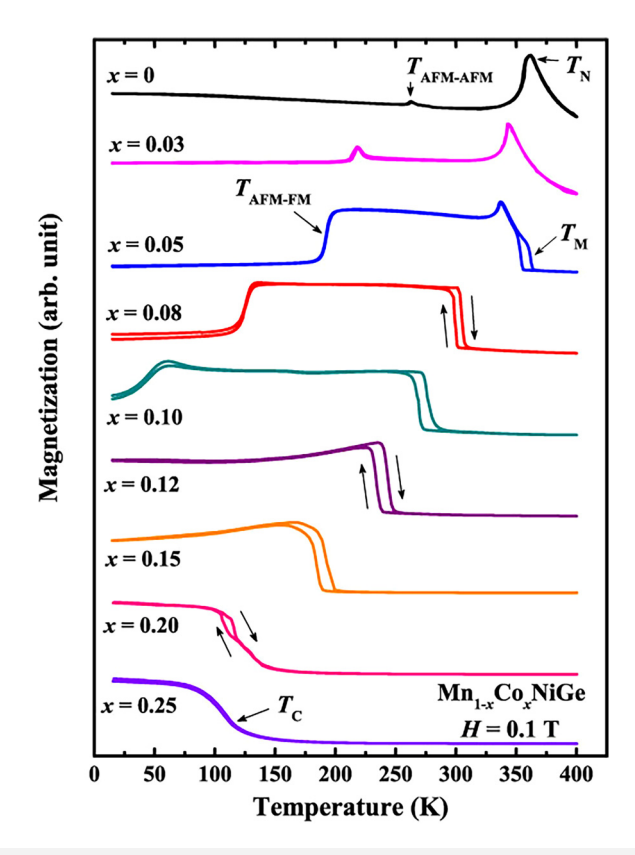


FIG. 3. Temperature-dependent magnetization of all Mn_{1-x}Co_xNiGe samples measured in an applied field of $H = 0.1 \,\mathrm{T}$ using ZFC and FCC protocols. The arrows indicate the direction of warming and cooling scans. As the Co concentration increased, the martensitic structural transition continuously shifted to a lower temperature and finally disappeared for x = 0.25.

be correlated with the strengthening of covalent bonds between the Ni and Ge atoms, and between the neighboring Mn-Mn atoms, similar to that observed in MnNiGe with Fe substituted for Mn.²² On the other hand, the magnetization in the martensite phase appreciably increased, suggesting that Co-doping establishes FM coupling in the original AFM martensite phase. As a consequence, the structural and magnetic transitions coupled to form a magnetostructural transition from the low-temperature FM orthorhombic to high-temperature PM hexagonal phase in samples with 0.05 < x < 0.20. The existence of thermal hysteresis between the heating and cooling curves in Fig. 3 confirms that the transitions are first order.

Upon further increase in Co content, a decoupling of the magnetic and structural transitions occurred in the sample with x = 0.20 with $T_C = 126$ and $T_M = 110$ K, respectively. Meanwhile, the structural transition completely disappeared for x = 0.25, leaving a magnetic transition at $T_C = 109 \text{ K}$ between the FM and PM states in the hexagonal phase. Here, the conversion of the magnetic structure from the AFM state to the FM state in the martensite phase can be attributed to ferromagnetic coupling introduced by Co substitution.³⁶ Since the Mn-Mn moments are considered to have an antiferromagnetic coupling,²⁹ the AFM interaction gradually diminishes if the doping of Co on the Mn site increases, establishing FM interaction in the martensite phase.

In addition to the MST, a transition (labeled as $T_{\mathrm{AFM-FM}}$ in Fig. 3) between the low-magnetization and high-magnetization orthorhombic phases was observed in the sample with x = 0.05 at T = 193 K. Taking into account a large difference in magnetization (ΔM) between the two magnetic states in the martensite phase, the transition is assumed to be an AFM-FM-like transition. The origin of this transition is likely rooted in the instability of the spiral AFM interaction in the stoichiometric MnNiGe martensite. As mentioned earlier, Co substitution introduces the FM coupling in the intrinsic AFM martensite phase by breaking the AFM coupling between the Mn atoms. As the FM interaction increases, competition occurs between the FM interaction and the originally present AFM exchange interaction, resulting in the AFM-FM-like transition. With increasing Co content, the AFM-FM-like transition continuously shifted to a lower temperature until it completely disappeared for x > 0.10. This indicates that the FM interaction induced by Co substitution completely dominated the AFM interaction in the martensite phase for x > 0.10. It is worth mentioning that the existence of the AFM-FM-like transition in the lowtemperature phase, in addition to a first-order magnetostructural transition between the FM orthorhombic and PM hexagonal phases, has not been reported previously in MnNiGe when Mn was substituted by Co. A similar observation has been reported in Mn_{1-x}Fe_xNiGe, where the AFM-FM-like transition is claimed to be a first-order magnetoelastic transition. However, in our results, the thermal hysteresis between the heating and cooling magnetization curves was not observed, suggesting that the AFM-FM-like and the arms of the curves was not observed. tion curves was not observed, suggesting that the AFM-FM-like transition is second order.

We further investigated the field-dependent behavior of the 8 phase transitions for low Co content samples. For this, temperature-dependent magnetization measurements were performed on the sample with x = 0.08 in applied magnetic fields of H = 0.1, 0.3, and 0.5 T, which are shown in Fig. 4. As the applied magnetic field increased, ΔM between the austenite and martensite phases increased significantly, shifting the magnetostructural transition slightly toward a higher temperature. On the other hand, the AFM-FM-like transition shifted to a lower temperature and broadened over a wider temperature range in the 0.3-T field, while it was nearly suppressed when the magnetization was measured in a field of 0.5 T. The observed large value of ΔM at the transition in the 0.5-T field indicates the domination of FM interactions over the intrinsic AFM martensite matrix in the martensite phase. This observation suggests that the AFM-FM-like transition is observed in a weak magnetic field and is gradually suppressed with increasing field (H > 0.5 T)

To understand the behavior of magnetic interactions in the martensite phase, isothermal magnetization measurements [M(H)]were performed on samples with x = 0.03, 0.05, 0.08, and 0.10 at ambient pressure at T = 2 K as shown in Fig. 5(a). The M(H) curves showed different behaviors depending on the Co concentration. A typical AFM behavior was observed in the sample with x = 0.03with a metamagnetic transition. The existence of the metamagnetic transition, the field-induced discontinuous jump

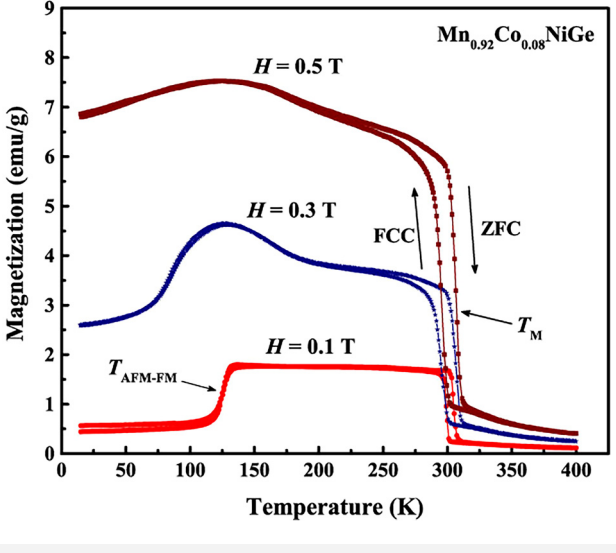


FIG. 4. The magnetization as a function of temperature for ${\rm Mn_{1-x}Co_xNiGe}$ (x = 0.08) in applied fields of 0.1, 0.3, and 0.5 T. The magnetization curves were measured using ZFC and FCC protocols.

magnetization, indicates the conversion of AFM alignment to a FM configuration [see Fig. 5(a)]. As the Co content increased, a clear evolution from the AFM state to the FM state was realized. This signifies that Co substitution in the Mn site results in FM interaction and gradually changes the magnetic structure of the martensite phase by breaking the original AFM spin alignment. Figure 5(b) shows the composition dependence of the critical field $(H_{\rm cr})$ at T=2 K. Here, the critical field is defined as the applied magnetic field that causes the onset of the metamagnetic transition, which is characterized by a peak in the dM/dH curves as displayed in the inset of Fig. 5(b). As the Co concentration increased, $H_{\rm cr}$ decreased almost linearly, indicating a weakening of the original AFM order in the martensite phase. These results are in agreement with the temperature-dependent magnetization measurements shown in Figs. 3 and 4.

Based on the heat flow (DSC), magnetization, and XRD measurements, a comprehensive structural and magnetic phase diagram as a function of Co concentration has been constructed, which is shown in Fig. 6. Here, the martensitic structural transition temperature (T_M) is defined as an average of the forward and reverse structural transition temperatures, which were determined from the derivative of the M-T curves with H = 0.1 T. For x = 0 and 0.03, those temperatures were determined from the DSC curves. Similarly, the magnetic transition temperatures (T_N/T_C) and $T_{AFM-AFM}/T_{AFM-FM}$) are defined as the inflection points in the M-T curves measured in a field of H = 0.1 T. In Fig. 6, it can be seen that $T_{
m M}$ continuously decreased with increasing Co content until it disappeared for x = 0.25. At the same time, $T_{AFM-AFM}/T_{AFM-FM}$ shifted to a lower temperature and then disappeared. The magnetic and structural transitions coexist to form a magnetostructural transition between the PM hexagonal and FM orthorhombic phases for 0.05 < x < 0.20 in a large temperature interval from 135 to 335 K.

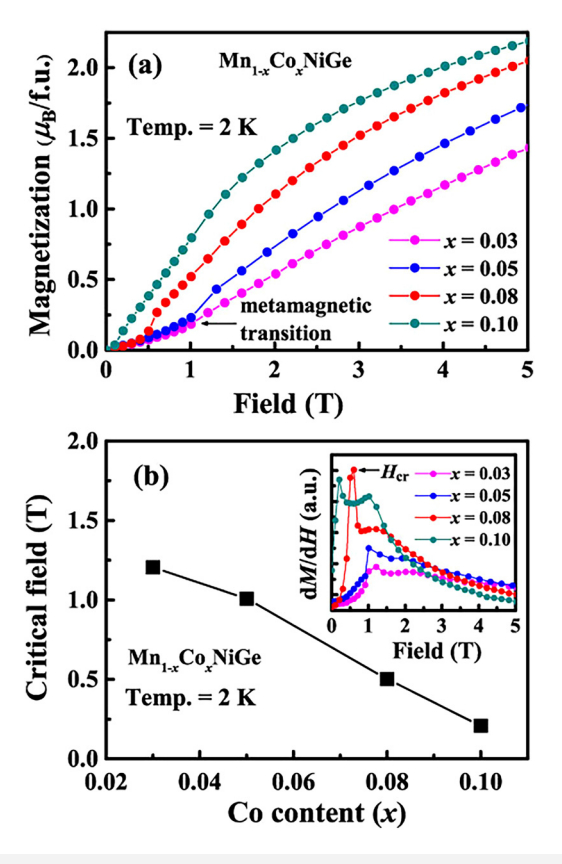


FIG. 5. (a) Isothermal magnetization curves of $Mn_{1-x}Co_xNiGe$ measured at T=2 K in fields up to 5 T at ambient pressure. (b) The critical field (H_{cr}) as a function of Co concentration in $Mn_{1-x}Co_xNiGe$ at T=2 K. The inset shows dM/dH as a function of the magnetic field, where H_{cr} is the critical field.

26 December 2024 02:28:1

B. Effects of hydrostatic pressure

Magnetization measurements on $Mn_{1-x}Co_xNiGe$ (x = 0.03, 0.05, 0.08, and 0.10) as a function of temperature were carried out under applied hydrostatic pressure. Figure 7 shows thermomagnetic data measured in a 0.1-T field using ZFC and FCC protocols at ambient pressure and under the specified pressure. The application of hydrostatic pressure shifted the martensitic structural transition toward a lower temperature. For x = 0.03, T_M decreased at a rate of $dT_{\rm M}/dP = -7.1$ K/kbar from T = 389 to 314 K. Similarly, it decreased at a rate of $dT_M/dP = -6.4 \text{ K/kbar from } T = 357 \text{ to } 293 \text{ K}$ in the sample with x = 0.05. Consequently, a pressure-formed magnetostructural transition from a low-temperature orthorhombic FM to a high-temperature hexagonal PM phase was observed at T = 314 K for x = 0.03 under a pressure of P = 10.6 kbar, while it was observed at T = 293 K for x = 0.05 with P = 10 kbar. Interestingly, the effect of pressure on the AFM-FM-like transition was opposite to that of the magnetic field (compare Figs. 4 and 7). Under hydrostatic pressure, the AFM-FM-like transition shifted toward higher temperature in both samples.

Moreover, decoupling of the magnetic and structural transitions was observed in the sample with x = 0.08 under a pressure of

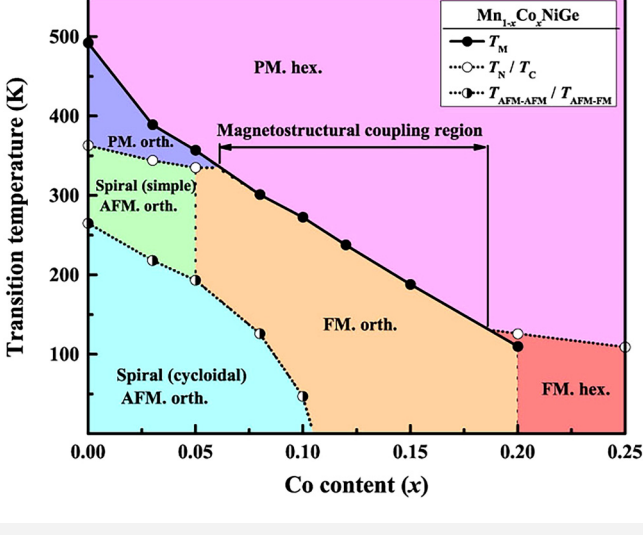


FIG. 6. A comprehensive magnetic and structural phase diagram for the $Mn_{1-x}Co_xNiGe$ system. The structural (T_M) and magnetic (T_N/T_C) and $T_{AFM-AFM}/T_{AFM-FM}$ transition temperatures were determined from DSC, XRD, and magnetization (with H=0.1 T) measurements. The terms "hex." and "orth." indicate the hexagonal and orthorhombic structures, respectively. A magnetostructural transition was realized in the range 0.05 < x < 0.20. The results for $x \ge 0.10$ are in good agreement with the phase diagram described in Ref. 36.

P = 11 kbar, where the martensitic structural transition occurred at $T_{\rm M} = 254 \, {\rm K}$ and the magnetic transition occurred at $T_{\rm C} = 183 \, {\rm K}$. Meanwhile, the first-order magnetostructural transition present at ambient pressure in the sample with x = 0.10 completely converted into a second-order magnetic transition under a pressure of P = 11 kbar, where the transition occurred at $T_C = 180 \text{ K}$ between the FM and PM states in the hexagonal phase. The disappearance of the structural transition, i.e., stabilization of the hexagonal phase, can be ascribed to the shortening of the Mn-Mn interlayer distance and strengthening of the covalent bond between Mn-Mn atoms due to the application of pressure.⁴⁷ A similar disappearance of the martensitic structural transition due to hydrostatic pressure has been observed in MnCoGe systems. 23,48 These results indicate that the martensitic structural transitions in the Mn_{1-x}Co_xNiGe system are highly sensitive to applied pressure, which is useful to maximize the contribution of the lattice to the MCE and suggests the possibility of large barocaloric effects.

To study the effect of pressure on the magnetic interactions in the low-temperature phase, we measured isothermal magnetization on samples with x=0.03, 0.05, 0.08, and 0.10 under the specified hydrostatic pressures at T=2 K, as shown in Fig. 8. Under hydrostatic pressure, the M(H) curves of the samples with x=0.03 and 0.05 show an AFM behavior with accompanying metamagnetic transitions. For both samples, the critical fields corresponding to the metamagnetic transitions slightly increased under hydrostatic pressure relative to that measured at ambient pressure. This is likely due to the pressure-induced shift of the AFM-FM-like transition to a higher temperature as observed in Fig. 7. A typical FM M(H) curve was observed in the samples with x=0.08 and 0.10 under

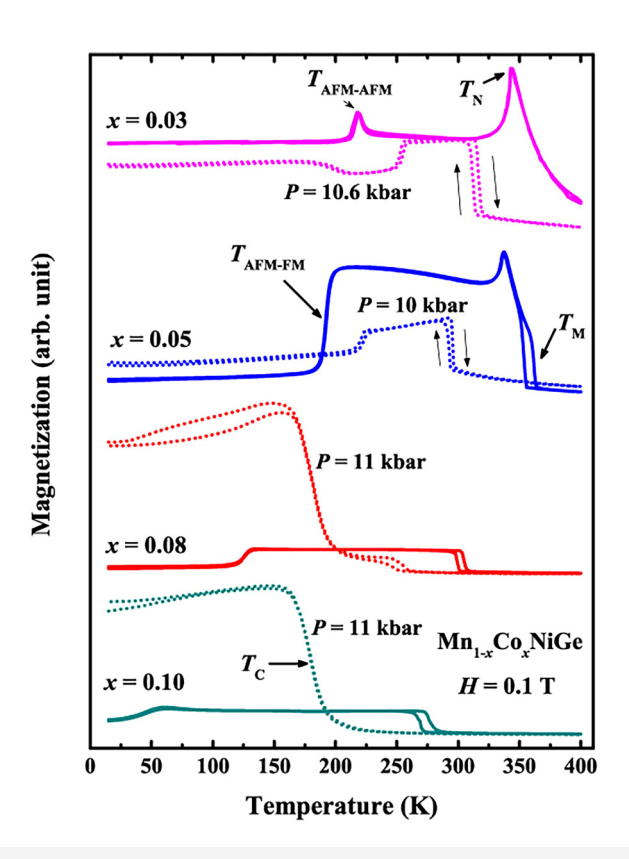


FIG. 7. The temperature-dependent magnetization of $Mn_{1-x}Co_xNiGe$ measured in an applied field of $H=0.1\,T$ using ZFC and FCC protocols. The solid lines and dashed lines represent measurements performed at ambient pressure and under the indicated hydrostatic pressures, respectively.

P=11 kbar, indicating that the application of pressure expedites the conversion of AFM into FM interaction in the martensite phase. These results are consistent with the temperature-dependent magnetization results, as shown in Fig. 7.

To evaluate the isothermal magnetic entropy change (ΔS_M) , a series of isothermal magnetization measurements in fields of up to 7 T were carried out as the temperature was stepped through the magnetostructural transition. To eliminate the history-dependent magnetic states at the magnetostructural transitions with thermal hysteresis, a "loop process method" was adopted. ^{49,50} In this method, the samples were heated to the PM austenite state and then cooled to the targeted measurement temperature under zero field before each isothermal magnetization measurement. The magnetic entropy changes were then determined from the magnetization isotherms using the thermodynamic relation,

$$\begin{split} \Delta S_M(T,\Delta H) &= \int_0^H \left(\frac{\partial M(T,H')}{\partial T}\right)_H dH' \\ &\cong \frac{1}{\Delta T} \left[\int_0^H M(T+\Delta T,H') dH' - \int_0^H M(T,H') dH'\right]. \end{split}$$

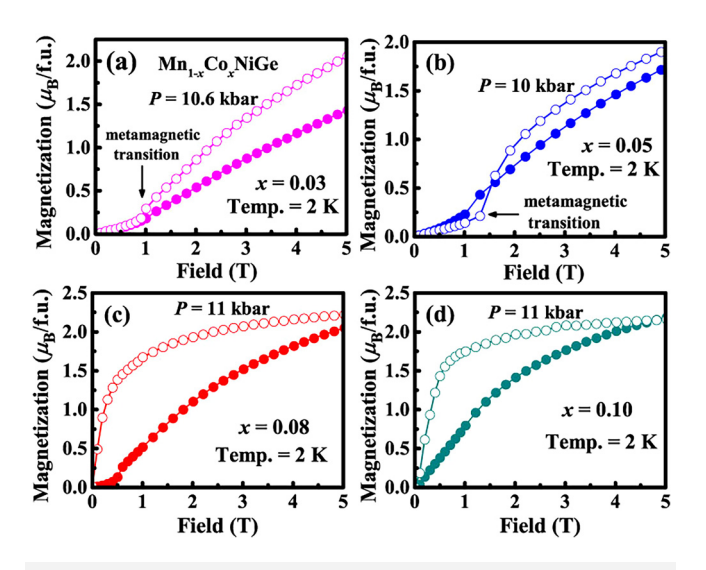


FIG. 8. Isothermal magnetization curves of $Mn_{1-x}Co_xNiGe$ with (a) x = 0.03, (b) x = 0.05, (c) x = 0.08, and (d) x = 0.10 measured at T = 2 K in fields up to 5 T. The solid and open circles represent the magnetization measurements performed at ambient pressure and under the indicated hydrostatic pressures, respectively.

Figure 9 shows the temperature-dependent magnetic entropy changes $(-\Delta S_M)$ of $Mn_{1-x}Co_xNiGe$ for field changes of $\Delta H = 2$ and 7 T at ambient pressure and under hydrostatic pressure. At ambient pressure, the sample with x = 0.08 shows the largest magnetic entropy change $(\Delta S_M = -56.2 \text{ J kg}^{-1} \text{ K}^{-1} \text{ for } \Delta H = 7 \text{ T})$ near room temperature, and its full width at half maximum of ΔS_M is $\delta_{FWHM} \cong 4.2 \text{ K}$. It also shows the largest relative cooling power $(RCP \approx 236 \text{ J/kg for a 7-T field change})$, which was estimated using $RCP = \Delta S_{max} \times \delta_{FWHM}$ for $\Delta H = 7$ T. Since the magnetic and structural transitions are not coupled in the sample with x = 0.03 at ambient pressure, it is expected to have a small magnetic entropy change, if measured. However, under a pressure of 10.6 kbar, it shows a large magnetic entropy change ($\Delta S_M = -80.3 \text{ J kg}^{-1} \text{ K}^{-1}$ for $\Delta H = 7 \text{ T}$) at T = 315 K with $\delta_{FWHM} \cong 3.6 \text{ K}$, and has a large relative cooling power ($RCP \approx 289 \text{ J/kg}$). Similarly, an enhancement in the magnetic entropy change by a factor of 5, from -14 to $-69 \,\mathrm{J\,kg^{-1}\,K^{-1}}$ for $\Delta H = 7 \,\mathrm{T}$ with $\delta_{FWHM} \cong 4.1 \,\mathrm{K}$ was observed in the sample with x = 0.05 when changing the pressure from 0 to 10 kbar. These enhancements can be attributed to the pressureformed, first-order magnetostructural transitions in these samples.

Moreover, it is reasonable to expect a reduction in the magnetic entropy change in the samples with x=0.08 and 0.10 under hydrostatic pressure due to a pressure-induced decoupling of the magnetic and structural transitions. These results demonstrate that, by adjusting the Co concentration and applying appropriate pressure, large tunable magnetic entropy changes can be obtained in the $\mathrm{Mn_{1-x}Co_xNiGe}$ system. Additionally, the high sensitivity of the martensitic structural transition to hydrostatic pressure $(\mathrm{d}T_\mathrm{M}/\mathrm{d}P \sim -7~\mathrm{K/kbar})$ suggests that pronounced barocaloric and magnetocaloric effects may both occur in this system.

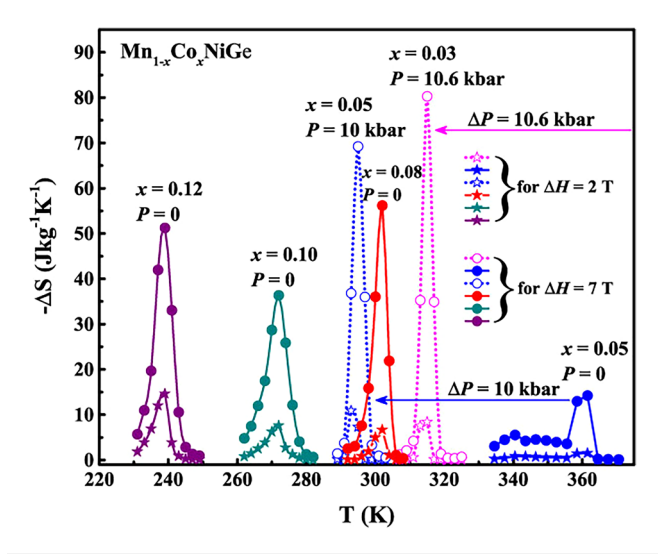


FIG. 9. The magnetic entropy changes (ΔS_M) of $\mathrm{Mn}_{1-x}\mathrm{Co}_x\mathrm{Ni}$ Ge as a function of temperature for $\Delta H=2$ and 7 T. The solid and open symbols represent measurements performed at atmospheric pressure (i.e., P=0) and under the indicated hydrostatic pressures, respectively. The arrows indicate the direction in which the peaks of ΔS_M shift due to the change in pressure. Since the magnetic and structural transitions are not coupled in the sample with x=0.03 at ambient pressure, ΔS_M is expected to be very small around $T_M=389$ K, if measured (not shown in the figure).

C. Effects of thermal quenching

We selected the sample with x = 0.03 for a thermal quenching study, where the as-cast ingots were annealed at different temperatures in evacuated quartz tubes followed by quenching in liquid nitrogen in order to stabilize the high-temperature, structural phase near room temperature. The intention was to form a coupled magnetostructural transition at room temperature. All samples and their quenching conditions are summarized in Table II.

Figure 10 shows the room temperature XRD patterns for all heat-treated samples. At room temperature, the reflections of samples SC800, Q800, Q900, Q1000, and Q1100 can be indexed as the TiNiSi-type orthorhombic phase, while the patterns of the sample Q1200 can be primarily indexed as the Ni₂In-type hexagonal phase with some traces of the orthorhombic phase, indicating

TABLE II. The quenching conditions of the sample with x = 0.03.

Composition	Label	Quenching temperature (°C)	Cooling process
x = 0.03	SC800	800	Slowly cooled
	Q800	800	Quenched
	O900	900	Quenched
	Q1000	1000	Quenched
	Q1100	1100	Quenched
	Q1200	1200	Quenched

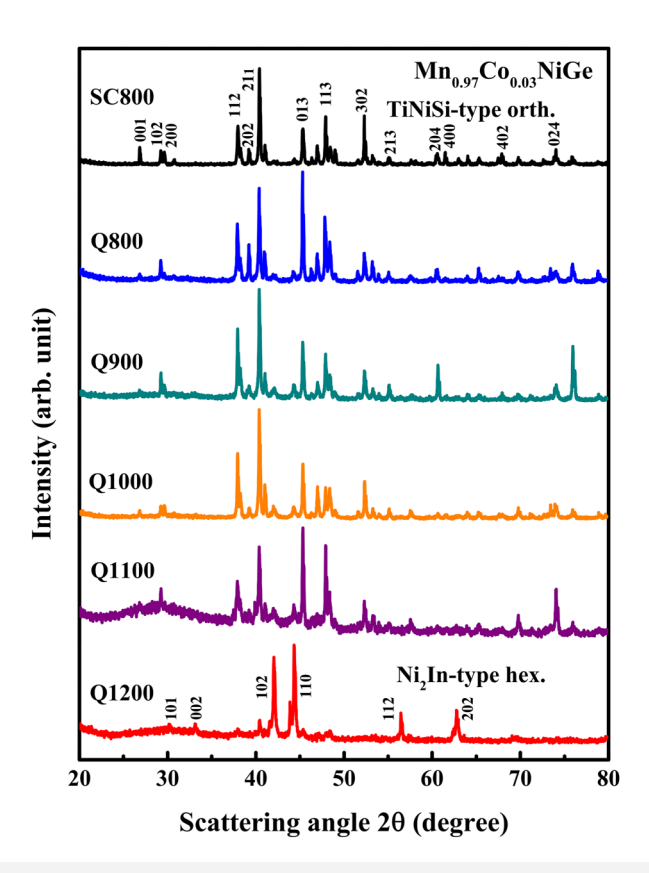


FIG. 10. Room temperature powder x-ray diffraction patterns for $Mn_{1-x}Co_xNiGe$ (x = 0.03) quenched from different temperatures. The increasing quenching temperature leads to the stabilization of the high-temperature Ni_2In -type hexagonal phase.

its structural transition is near room temperature. With these results, it can be expected that a rapid cooling from a temperature >1200 °C lowers the structural transition below room temperature, stabilizing the high-temperature hexagonal phase. Furthermore, the Rietveld refinement results, as tabulated in Table III, show that the lattice parameters and cell volumes per formula unit in the orthorhombic phase decrease continuously with increasing quenching temperature. Meanwhile, similar results were observed with increasing Co concentration in $Mn_{1-x}Co_xNiGe$ (see Fig. 1 and Table I). Therefore, it can be concluded that the increasing quenching temperature leads to the reduction in cell volume and the lowering of structural transitions, $^{23,48}_{23,48}$ which are analogous to the effects of Co-doping in $Mn_{1-x}Co_xNiGe$.

To explore the effect of thermal quenching on the magnetization and phase transitions, temperature-dependent magnetization was measured for all heat-treated samples in a field of 0.1 T using field-cooled-cooling (FCC) and field-cooled-warming (FCW) protocols as shown in Fig. 11. For the sample that was slowly cooled from 800 °C (SC800), DSC data showed a martensitic structural transition occurring at $T_{\rm M}=389~{\rm K}$ (see Fig. 2), while the magnetization measurement displayed a sharp peak associated with the

TABLE III. The lattice parameters and cell volumes per formula unit obtained from Rietveld refinements of the x-ray powder diffraction data of all heat-treated Mn_{0.97}Co_{0.03}NiGe samples measured at room temperature.

Sample	Major phase	a (Å)	b (Å)	c (Å)	Vol./f.u. (Å ³)
SC800	Orth.	6.028	3.755	7.092	40.13
Q800	Orth.	6.026	3.754	7.087	40.08
Q900	Orth.	6.022	3.756	7.084	40.06
Q1000	Orth.	6.019	3.753	7.080	39.98
Q1100	Orth.	6.017	3.752	7.077	39.94
Q1200	Hex.	4.086	4.086	5.409	39.10

AFM–PM transition at $T_{\rm N}$ = 344 K (see Fig. 11). Besides these, a small peak related to an AFM–AFM transition was observed at $T_{\rm AFM-AFM}$ = 217 K. As the annealing/quenching temperature increased, $T_{\rm M}$ decreased continuously to room temperature. Concurrently, the magnetization of the low-temperature phase increased significantly.

For the sample quenched from 900 °C (Q900), a magneto-structural transition between the PM hexagonal and high-

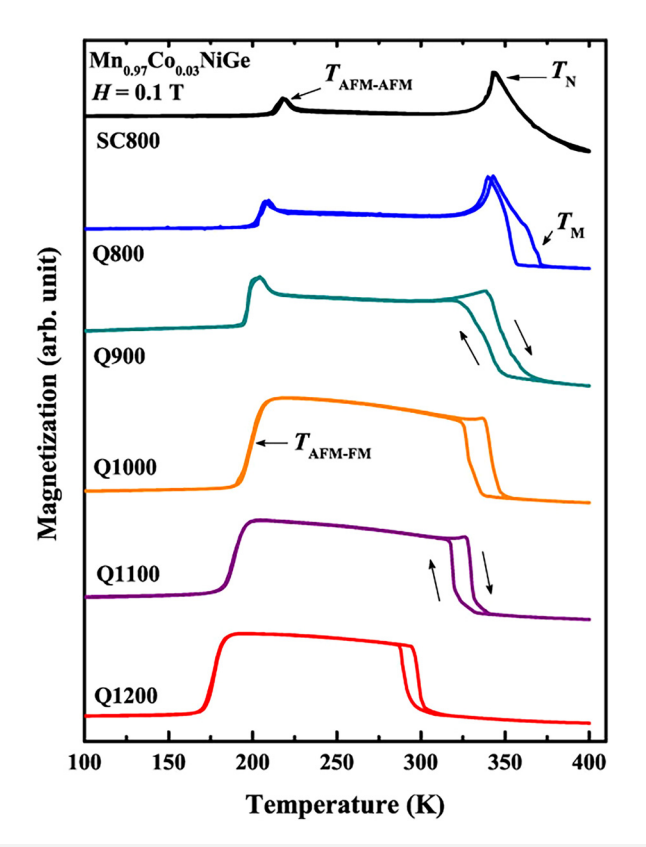


FIG. 11. Magnetization as a function of temperature for $Mn_{1-x}Co_xNiGe$ (x = 0.03) quenched from different temperatures. The magnetization curves were measured in a magnetic field of 0.1 T using FCC and FCW protocols, where the arrows indicate the direction of the heating and cooling paths.

magnetization orthorhombic phases was observed at $T_{\rm M} = 341 \, {\rm K}$ (Fig. 11). The presence of thermal hysteresis indicates that the transitions are first order. Meanwhile, an additional transition between the low-magnetization and high-magnetization orthorhombic phases was observed at T = 198 K, which is assumed to be an AFM-FM-like transition. These results suggest that the thermal quenching not only shifts the martensitic structural transition to lower temperature, thereby forming a metastable phase, but also gradually establishes ferromagnetic coupling in the intrinsic AFM martensite phase, where a competition may occur between induced-FM and intrinsic AFM exchange interactions leading to the evolution of an AFM-FM-like transition, similar to the behavior observed for Co variation as described earlier. Moreover, the magnetostructural transition was observed near room temperature when the sample was quenched from 1200 °C (Q1200), which may be further shifted below room temperature with increasing quenching temperature. Our results provide clear evidence that thermal processing can tune the magnetic and structural transitions over a wide range of temperatures in the MnNiGe-based system without chemical modifications or application of physical pressure. Similar results of magnetostructural transitions being formed by thermal treatments have been reported in MnCoGe and MnNiSi systems.4

Figure 12 shows the structural and magnetic phase diagrams of Mn_{0.97}Co_{0.03}NiGe as a function of quenching temperature. The magnetic and structural transition temperatures were obtained from the magnetization (with H = 0.1 T), DSC, and XRD measurements as described earlier. It can be seen in Fig. 12 that $T_{\rm M}$ decreases continuously with increasing quenching temperature. For the samples quenched from 900 to 1200 °C, the martensitic structural transition coincides with the magnetic transition, thereby

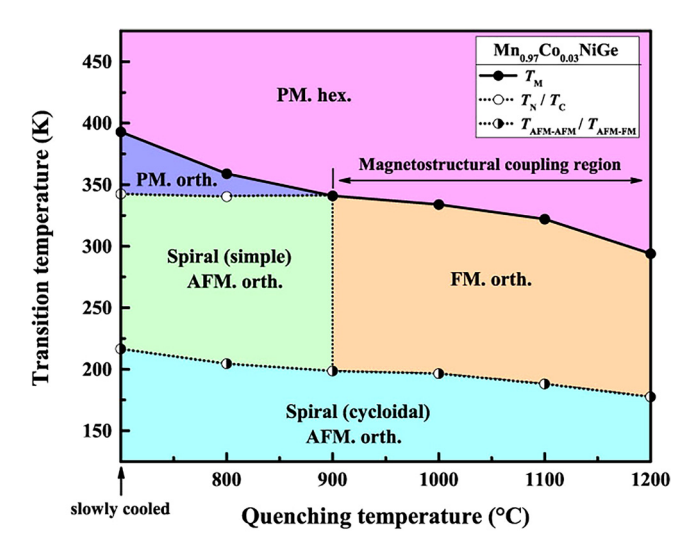


FIG. 12. A phase diagram illustrating the effects of quenching temperature on the structural $(T_{\rm M})$ and magnetic $(T_{\rm N}/T_{\rm C})$ and $T_{\rm AFM-AFM}/T_{\rm AFM-FM}$ transition temperatures of Mn_{0.97}Co_{0.03}NiGe. These transition temperatures were determined from DSC, XRD, and magnetization (with H = 0.1 T) measurements.

forming a magnetostructural transition between the FM orthorhombic and PM hexagonal phases in a temperature interval from 294 to 341 K. This behavior is promising for practical applications because the desired caloric effects can be adjusted over a wide temperature range around room temperature.

We further investigated the effect of thermal quenching on magnetic interactions in the low-temperature phase. Isothermal magnetization measurements of quenched samples were performed at T = 2 K in fields up to 5 T, the data of which are shown in Fig. 13. The magnetization curves of all the samples show a typical AFM behavior with metamagnetic transitions induced by a magnetic field. These metamagnetic transitions are associated with the transition from a spiral AFM to a FM configuration. As the quenching temperature increased, the critical field at 2 K continuously decreased from 1.2 T for SC800 to 0.8 T for Q1200 (see the inset in Fig. 13). The decrease in the critical field signifies a weakening of the AFM interaction in the martensite phase. Therefore, it can be concluded that increasing the quenching temperature strengthens the FM interaction in the low-temperature phase.

Figure 14 shows the temperature-dependent isothermal magnetic entropy changes for $\Delta H = 2$, 5, and 7 T for the samples quenched from 1100 (Q1100) and 1200 °C (Q1200). The ΔS_M values were estimated from the magnetization isotherms measured through the magnetostructural transitions following the loop process method as described earlier. The results show that both samples have comparable magnitudes of the magnetic entropy changes, but their peaks occur at different temperatures. In the sample Q1100, the maximum ΔS_M for 7-T field change is $\approx -51.2 \,\mathrm{J \, kg^{-1} \, K^{-1}}$ at 327 K, and its full width at half maximum of the entropy is $\delta_{FWHM} \cong 2.5 \,\mathrm{K}$, while the corresponding values in the sample Q1200 are $\Delta S_M = -56.5 \,\mathrm{L \, kg^{-1} \, K^{-1}}$ at 295 K and the sample Q1200 are $\Delta S_M = -56.5 \text{ J kg}^{-1} \text{ K}^{-1}$ at 295 K and the sample Q1200 are $\Delta S_M = -30.5$ kg K at 293 K and $S_M = -30.5$ kg K at 293 K at samples are nearly equal, i.e., RCP = -128 and -130 J/kg for a 7-T $\frac{82}{2}$

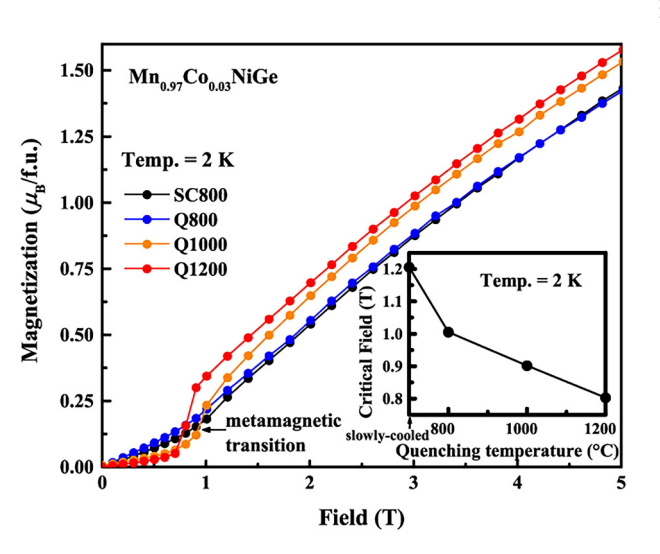


FIG. 13. Isothermal magnetization curves at $T = 2 \,\mathrm{K}$ in fields up to $5 \,\mathrm{T}$ for $Mn_{1-x}Co_xNiGe$ (x = 0.03) quenched from different temperatures. The inset shows the critical fields (H_{cr}) determined from the dM/dH curves

70

60

50

40

30

20

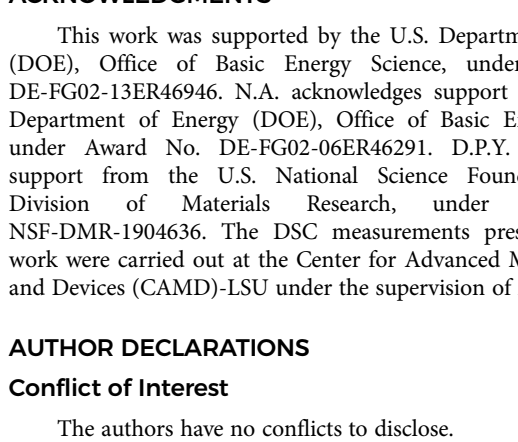
280

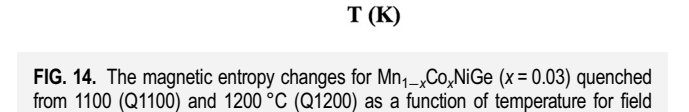
changes of 2, 5, and 7 T.

 $\Delta H = 5 \text{ T}$

290

Q1200





310

320

300

Mn_{0.97}Co_{0.03}NiGe

Q1100

 $\Delta H = 5 \text{ T}$

340

330

field change for Q1100 and Q1200, respectively. Note that the observed maximum ΔS_M values for Q1100 and Q1200 are comparable to or larger than those reported for most MnTX systems. 29,33,34,55 Therefore, it can be concluded that thermal processing can act as an effective method to tailor the magnetostructural transition over a wide range of temperatures, which can enhance the magnetocaloric properties of the MnNiGe-based systems.

IV. CONCLUSIONS

In summary, the magnetic, structural, and magnetocaloric properties of Mn_{1-x}Co_xNiGe as a function of Co concentration, applied pressure, and quenching temperature were systematically investigated. Substituting Co for Mn resulted in the formation of a first-order magnetostructural transition between the FM orthorhombic and PM hexagonal phases over a large temperature interval of $135 \text{ K} \le T \le 335 \text{ K}$ in samples with 0.05 < x < 0.20. Interestingly, an additional AFM-FM-like transition was observed in the martensite phase of low Co content samples ($x \le 0.10$), which was gradually suppressed with an increasing Co content (x > 0.10) or magnetic field (H > 0.5 T). Furthermore, the application of hydrostatic pressure or thermal quenching shifted the martensitic structural transition toward a lower temperature and formed coupled, magnetostructural transitions near room temperature in appropriately Co-substituted samples, which resulted in large magnetic entropy changes and relative cooling powers. Moreover, the high sensitivity of the martensitic structural transition to applied hydrostatic pressure suggests the potential for pronounced barocaloric effects, which leads to the possibility of obtaining multicaloric (barocaloric and magnetocaloric) effects in a single material. These results demonstrate that atomic substitution, application of pressure, and thermal quenching, and a combination

of these methods, can be used to tailor the functional properties in the MnNiGe-based system.

ACKNOWLEDGMENTS

This work was supported by the U.S. Department of Energy (DOE), Office of Basic Energy Science, under Award No. DE-FG02-13ER46946. N.A. acknowledges support from the U.S. Department of Energy (DOE), Office of Basic Energy Science, under Award No. DE-FG02-06ER46291. D.P.Y. acknowledges support from the U.S. National Science Foundation (NSF), Award NSF-DMR-1904636. The DSC measurements presented in this work were carried out at the Center for Advanced Microstructures and Devices (CAMD)-LSU under the supervision of A. Roy.

Author Contributions

Tej Poudel Chhetri: Conceptualization (equal); Formal analysis (equal); Investigation (equal); Methodology (equal); Software (equal); Validation (equal); Visualization (equal); Writing - original draft (equal). Jing-Han Chen: Methodology (equal); Writing review and editing (equal). Anthony T. Grant: Methodology (equal); Writing – review and editing (equal). David P. Young: Funding acquisition (equal); Methodology (equal); Resources (equal); Writing – review and editing (equal). Igor Dubenko: Writing – review and editing (equal). Saikat Talapatra: Writing – $\frac{6}{5}$ review and editing (equal). Naushad Ali: Funding acquisition (equal); Resources (equal); Writing – review and editing (equal). Shane Stadler: Funding acquisition (equal); Investigation (equal); Project administration (equal); Resources (equal); Supervision (equal); Writing - review and editing (equal).

DATA AVAILABILITY

The data that support the findings of this study are available from the corresponding author upon reasonable request.

REFERENCES

¹K. Ullakko, J. K. Huang, C. Kantner, R. C. O'Handley, and V. V. Kokorin, Appl. Phys. Lett. 69, 1966 (1996).

²R. Kainuma, Y. Imano, W. Ito, Y. Sutou, H. Morito, S. Okamoto, O. Kitakami, K. Oikawa, A. Fujita, T. Kanomata, and K. Ishida, Nature 439, 957 (2006).

³V. K. Pecharsky and K. A. Gschneidner, Jr., Phys. Rev. Lett. 78, 4494 (1997).

⁴H. Wada and Y. Tanabe, Appl. Phys. Lett. **79**, 3302 (2001).

⁵J. Liu, T. Gottschall, K. P. Skokov, J. D. Moore, and O. Gutfleisch, Nat. Mater. 11, 620 (2012).

⁶S. Y. Yu, Z. H. Liu, G. D. Liu, J. L. Chen, Z. X. Cao, G. H. Wu, B. Zhang, and X. X. Zhang, Appl. Phys. Lett. 89, 162503 (2006).

⁷C. Biswas, R. Rawat, and S. R. Barman, Appl. Phys. Lett. 86, 202508 (2005).

⁸A. Fujita, S. Fujieda, Y. Hasegawa, and K. Fukamichi, Phys. Rev. B **67**, 104416

⁹F. Hu, B. Shen, J. Sun, Z. Cheng, G. Rao, and X. Zhang, Appl. Phys. Lett. 78, 3675 (2001).

- ¹⁰J. Lyubina, O. Gutfleisch, M. D. Kuz'min, and M. Richter, J. Magn. Magn. Mater. **320**, 2252 (2008).
- ¹¹O. Tegus, E. Brück, K. H. J. Buschow, and F. R. de Boer, Nature **415**, 150 (2002).
- 12 F. Guillou, G. Porcari, H. Yibole, N. van Dijk, and E. Brück, Adv. Mater. 26, 2671 (2014).
- 13Y. Sutou, Y. Imano, N. Koeda, T. Omori, R. Kainuma, K. Ishida, and K. Oikawa, Appl. Phys. Lett. 85, 4358 (2004).
- ¹⁴S. Stadler, M. Khan, J. Mitchell, N. Ali, A. M. Gomes, I. Dubenko, A. Y. Takeuchi, and A. P. Guimarães, Appl. Phys. Lett. 88, 192511 (2006).
- 15T. Krenke, E. Duman, M. Acet, E. F. Wassermann, X. Moya, L. Mañosa, A. Planes, F. Suard, and B. Ouladdiaf, Phys. Rev. B 75, 104414 (2007)
- A. Planes, E. Suard, and B. Ouladdiaf, Phys. Rev. B 75, 104414 (2007).

 16V. D. Buchelnikov and V. V. Sokolovskiy, Phys. Metals Metallogr. 112, 633 (2011).

 17T. Gottschall, K. P. Skokov, B. Frincu, and O. Gutfleisch, Appl. Phys. Lett. 106, 021901 (2015).
- ¹⁸M. Khan, N. Ali, and S. Stadler, J. Appl. Phys. **101**, 053919 (2007).
- ¹⁹A. K. Pathak, M. Khan, I. Dubenko, S. Stadler, and N. Ali, Appl. Phys. Lett. 90, 262504 (2007).
- ²⁰N. T. Trung, L. Zhang, L. Caron, K. H. J. Buschow, and E. Brück, Appl. Phys. Lett. 96, 172504 (2010).
- ²¹T. Samanta, I. Dubenko, A. Quetz, S. Stadler, and N. Ali, Appl. Phys. Lett. 101, 242405 (2012).
- ²²A. Biswas, A. K. Pathak, N. A. Zarkevich, X. Liu, Y. Mudryk, V. Balema, D. D. Johnson, and V. K. Pecharsky, Acta Mater. 180, 341 (2019).
- ²³J.-H. Chen, A. Trigg, T. Poudel Chhetri, D. P. Young, I. Dubenko, N. Ali, and S. Stadler, J. Appl. Phys. 127, 213901 (2020).
- ²⁴W. Bazela, A. Szytuła, J. Todorović, Z. Tomkowicz, and A. Zięba, Phys. Status Solidi A 38, 721 (1976).
- ²⁵V. Johnson, <u>Inorg. Chem.</u> **14**, 1117 (1975).
- ²⁶H. Fjellvåg and A. F. Andresen, J. Magn. Magn. Mater. **50**, 291 (1985).
- 27S. Nizioł, A. Wesełucha, W. Bażela, and A. Szytuła, Solid State Commun. 39, 1081 (1981).
- ²⁸S. Nizioł, A. Bombik, W. Bażela, A. Szytuła, and D. Fruchart, J. Magn. Magn. Mater. 27, 281 (1982).
- ²⁹E. Liu, W. Wang, L. Feng, W. Zhu, G. Li, J. Chen, H. Zhang, G. Wu, C. Jiang, H. Xu, and F. de Boer, Nat. Commun. 3, 873 (2012).
- ³⁰J. Liu, Y. Gong, G. Xu, G. Peng, I. A. Shah, N. ul Hassan, and F. Xu, Sci. Rep. 6, 23386 (2016).
- ³¹C. L. Zhang, Z. D. Han, B. Qian, H. F. Shi, C. Zhu, J. Chen, and T. Z. Wang, J. Appl. Phys. 114, 153907 (2013).
- ³²C. Zhang, D. Wang, Q. Cao, S. Ma, H. Xuan, and Y. Du, J. Phys. D: Appl. Phys. 43, 205003 (2010).
- ⁵³T. Samanta, I. Dubenko, A. Quetz, S. Temple, S. Stadler, and N. Ali, Appl. Phys. Lett. **100**, 052404 (2012).

- ³⁴A. Quetz, T. Samanta, I. Dubenko, M. J. Kangas, J. Y. Chan, S. Stadler, and N. Ali, J. Appl. Phys. **114**, 153909 (2013).
- 35J. Liu, Y. Gong, Y. You, X. You, B. Huang, X. Miao, G. Xu, F. Xu, and E. Brück, Acta Mater. 174, 450 (2019).
- ³⁶E. K. Liu, H. G. Zhang, G. Z. Xu, X. M. Zhang, R. S. Ma, W. H. Wang, J. L. Chen, H. W. Zhang, G. H. Wu, L. Feng, and X. X. Zhang, Appl. Phys. Lett. 102, 122405 (2013).
- 37Y. Kuang, B. Yang, X. Hao, H. Xu, Z. Li, H. Yan, Y. Zhang, C. Esling, X. Zhao, and L. Zuo, J. Magn. Magn. Mater. 506, 166782 (2020).
- ⁵⁸C. L. Zhang, D. H. Wang, Q. Q. Cao, Z. D. Han, H. C. Xuan, and Y. W. Du, Appl. Phys. Lett. **93**, 122505 (2008).
- ³⁹S. Anzai and K. Ozawa, Phys. Rev. B **18**, 2173 (1978).
- ⁴⁰A. Taubel, T. Gottschall, M. Fries, T. Faske, K. P. Skokov, and O. Gutfleisch, J. Phys. D: Appl. Phys. 50, 464005 (2017).
- ⁴¹Y. Kuang, J. Qi, H. Xu, B. Yang, B. Li, Z. Li, H. Yan, Y. Zhang, C. Esling, X. Zhao, and L. Zuo, Scr. Mater. **200**, 113908 (2021).
- ⁴²A. P. Sivachenko, V. I. Mityuk, V. I. Kamenev, A. V. Golovchan, V. I. Val'kov, and I. F. Gribanov, Low Temp. Phys. **39**, 1051 (2013).
- 43Y. Li, Q. Zeng, Z. Wei, E. Liu, X. Han, Z. Du, L. Li, X. Xi, W. Wang, S. Wang, and G. Wu, Acta Mater. 174, 289 (2019).
- 44H. M. Rietveld, J. Appl. Cryst. 2, 65 (1969).
- ⁴⁵B. H. Toby, J. Appl. Cryst. **34**, 210 (2001).
- 46 K. Xu, Z. Li, E. Liu, H. Zhou, Y. Zhang, and C. Jing, Sci. Rep. 7, 41675 (2017).
- ⁴⁷R.-R. Wu, L.-F. Bao, F.-X. Hu, H. Wu, Q.-Z. Huang, J. Wang, X.-L. Dong, G.-N. Li, J.-R. Sun, F.-R. Shen, T.-Y. Zhao, X.-Q. Zheng, L.-C. Wang, Y. Liu, W.-L. Zuo, Y.-Y. Zhao, M. Zhang, X.-C. Wang, C.-Q. Jin, G.-H. Rao, X.-F. Han, and B.-G. Shen, Sci. Rep. 5, 18027 (2015).
 ⁴⁸J.-H. Chen, T. Poudel Chhetri, C.-K. Chang, Y.-C. Huang, D. P. Young,
- ⁴⁸J.-H. Chen, T. Poudel Chhetri, C.-K. Chang, Y.-C. Huang, D. P. Young, I. Dubenko, S. Talapatra, N. Ali, and S. Stadler, J. Appl. Phys. **129**, 215108 (2021).
- ⁴⁹L. Caron, Z. Q. Ou, T. T. Nguyen, D. T. Cam Thanh, O. Tegus, and E. Brück, J. Magn. Magn. Mater. **321**, 3559 (2009).
- 50J.-H. Chen, A. Us Saleheen, P. W. Adams, D. P. Young, N. Ali, and S. Stadler, J. Appl. Phys. 123, 145101 (2018).
- ⁵¹C. L. Zhang, Y. G. Nie, H. F. Shi, E. J. Ye, Z. D. Han, and D. H. Wang, J. Magn. Magn. Mater. **469**, 437 (2019).
- 52 K. Noguchi, R. Kobayashi, Y. Mitsui, R. Y. Umetsu, J. Gouchi, Y. Uwatoko, and K. Koyama, J. Magn. Magn. Mater. 499, 166199 (2020).
- ⁵³J.-H. Chen, T. Poudel Chhetri, A. Us Saleheen, D. P. Young, I. Dubenko, N. Ali, and S. Stadler, <u>Intermetallics</u> 112, 106547 (2019).
- ⁵⁴J.-H. Chen, A. Us Saleheen, S. K. Karna, D. P. Young, I. Dubenko, N. Ali, and S. Stadler, J. Appl. Phys. **124**, 203903 (2018).
- ⁵⁵E. K. Liu, Z. Y. Wei, Y. Li, G. D. Liu, H. Z. Luo, W. H. Wang, H. W. Zhang, and G. H. Wu, Appl. Phys. Lett. **105**, 062401 (2014).